Kinetic Investigation on Solvating Alkylamine Hofmann Elimination over Brønsted Acidic Zeolites

Han Chen [1] and Omar A. Abdelrahman [2*]

[1] Chemical Engineering, University of Massachusetts Amherst, 686 N. Pleasant Street, Amherst, MA 01003
[2] Chemical and Biomolecular Engineering, University of Houston, Houston, TX 77204

*Corresponding Author: oabdel@uh.edu

Keywords: Hofmann Elimination, Zeolite, Solvent Effect, Brønsted Acid Site, Cooperative Adsorption

Abstract. The presence of solvents can significantly alter the reaction kinetics of catalytic conversions, yet the mechanisms of the solvent effect remain widely debated and could greatly vary between different chemistries. We use vapor phase Hofmann elimination of tert-butylamine (TBA) to systematically investigate how solvents participate catalyzed reaction over Brønsted acid sites of solid acid catalysts and affect a catalytic cycle. Twenty commonly used organic and inorganic solvents were tested to investigate the relationship between solvent identity and their influence on reaction kinetics. Kinetic measurements showed a significant and reversible inhibition in rates of Hofmann elimination in the presence of every tested solvent, with the degrees of reduction vary from less than 10% for non-polar solvents (carbon dioxide, benzene, hexane) to more than 90 % (methanol, ethanol, 1-propanol, acetonitrile), which was found to exhibit a roughly linear against the molecular dipole moment of solvents. Additionally, the degree of reduction is not affected by the size of molecule as the carbon chain length increases, but is negatively related to the degree of substitution by alkyl group on the α-carbon as well as halogen atom on the β-carbon. Despite the significant kinetic inhibition and a 30 kJ mol^{-1} increase in the measured apparent activation energies, the temperature programmed surface reaction profiles performed with pre-adsorbed TBA with feeding of acetonitrile and methanol showed no change in the peak temperature from the catalyst without solvent feed. Cooperative adsorption complex formed between the surface tert-butylammonium and solvent molecule adsorbed on a neighboring framework oxygen, which is far less reactive towards Hofmann elimination, is proposed to be responsible for the observed rate inhibition. Also, the stability of adsorption complex formation is found to be affected by the proton affinity of solvent, as revealed by the kinetic modeling of experimental rate measurements.

1. Introduction. Solid acid catalysts, such as aluminosilicate zeolites, have been widely used in a variety of catalytic conversions, including sugar isomerization,[1, 2] alcohol dehydration,[3, 4] aldol condensation,[5] aromatic isomerization,[6] alkene epoxidation,[7] and many more. For these catalytic synthesis strategies, the use of solvent(s) is frequently involved. The presence of solvent in the reaction system is widely acknowledged to dramatically affect the reaction kinetics.[8] Water is one

of the most commonly used solvents, and the solvent effect of water on heterogeneous catalysis has been studied for decades. For example, the presence of water enhances the rate of acetone and acetic acid synthesis during propylene oxidation over vanadium-molybdenum catalyst.[9] In addition, the yields of CO_2 and propylene are dramatically increased with a co-fed of water vapor during furan catalytic pyrolysis over ZSM-5.[10] In contrast, water inhibits both the monomeric and dimeric dehydration of ethanol, leading to -1 reaction order with respect to water partial pressure.[11] Apart from water, organic solvents could also significantly promote the synthesis process. Research led by Dumesic showed that γ-valerolactone (GVL) significantly increases the rate of Brønsted acid-catalyzed production of furfural from xylose, which outperformed the use of water.[12] The promotional effect was attributed to the stabilization of Brønsted acidic proton relative to the protonated transition state by the polar aprotic solvent. In another case of glucose or fructose dehydration to 5-hydroxymethylfurfural (HMF), the use of pure water as solvent is avoided due to the side reaction between water and HMF to produce levulinic acid and formic acid.[13] Investigation by Nikolla et al. shows that for the Sn-Beta zeolite-catalyzed glucose dehydration, the use of biphasic system of water/1-butanol and water/tetrahydrofuran result in both higher conversion and selectivity towards HMF formation than the use of aqueous system.[14] These previous works manifest the weakness of water as solvent and the broad range of solvents applicable for the solid acid-catalyzed reactions.

The proper selection of solvent for the desired solvation effect upon the catalytic conversion has long been a critical consideration during the design of synthesis strategies. The physical and chemical properties of the solvent dictate its interaction with reactants, kinetic relevant transition state, as well as the active sites of the catalyst. Bertero and coworkers examined six solvents with varying polarities and found that the rate of citronellal isomerization/cyclization to isopulegol over SiO_2-Al_2O_3 was highest using the weakly polar chloroform.[15] Additionally, the effect of solvent could also be affected by the changes in confinement size, surface hydrophilicity/hydrophobicity, etc. Turnover rates of 1-hexene epoxidation over Ti-incorporated MFI zeolite differ by 1000-fold across various combination of solvent and silanol defect densities, as showed by Torres et al.[16] The use of cosolvent system further adds complexity to the applications. The major production of Brønsted acid-catalyzed 1,2-propanediol dehydration, carried out by Chew and colleagues, was found to be propanal in the 1,4-dioxane/water cosolvent environment, while in the dimethyl sulfoxide/water cosolvent environment the major product became acetone.[17] Therefore, the choices of solvents for the reaction system offer additional manipulation for the reaction kinetics.

To obtain guidance for the choice of best solvent for the catalytic conversion, it is important to understand how solvent affects the reaction kinetics. Generally, solvents affect solid acid-catalyzed reactions through adsorption on active sites,[18] altering catalyst/active site structure,[19, 20] and solvating reactants and transition states.[21] The rate inhibition by water against 1-propanol dehydration over H-MFI zeolite was attributed to the more stabilized adsorbed water-propanol dimers compared to their monomers leading to an increased reaction barrier.[3] Bates et al. proposed similar formation of water-ethanol dimer during ethanol dehydration over H-BEA, but they further investigated the contribution from the protonated water cluster network and also the influence of pore confinement environment on solvation effects.[11] Similarly, Cordon and coworkers showed that during the aqueous-phase isomerization of glucose over Sn-Beta zeolites, high silanol defect

density inside the pore would lead to stabilization of the extended hydrogen-bonded water networks, which entropically destabilize the transition states of reaction and lower the turnover rates.[22]

It can be seen that due to the complex interaction between reactants, solvents and solid acid catalysts, the mechanism of solvent affecting the reaction rate is usually interpreted for the specific chemical reaction over certain catalysts. Unfortunately, due to the limited manpower and the complex reaction system, most studies only focus on solvation mechanism of one or a few selected solvents, and thus a generalized solvation effect or mechanism is lacked. Moreover, many researchers adopted liquid-phase reactions when deciphering the effect of solvent, and faced the challenge of the highly non-ideal thermodynamics of the liquid phase. In some research work, probe chemistries that already involve water as a reactant or product, such as alcohol dehydration which is frequently used to probe the activity of acidic sites, were used for investigating the effect of solvents including water, which could mask how water could independently affect the kinetics.

To tackle the potential challenges in interpreting the solvent effect over solid acid catalysts, we previously proposed the use of vapor-phase primary alkylamine Hofmann elimination as probe chemistry to investigate the effect of water over H-ZSM-5 zeolite.[23] The advantages of this probe chemistry include less thermodynamic non-ideality in the vapor phase, exclusive Brønsted acid-catalyzed reaction, well-characterized stoichiometric adsorption of reactant, and most importantly, water not being involved as reactant, product or solvent. We observed a significant negative impact on the rate of Hofmann elimination when water vapor was co-fed with the reactant, tert-butylamine (TBA), while such rate inhibition was completely void once water was removed from the feed. The extent of inhibitory effect depends on the partial pressure of water as well as reaction temperature, but was unaffected by TBA partial pressure or the Al content of zeolites. A combination of kinetic measurements, in-situ spectroscopy, and temperature-programmed investigation revealed that the rate inhibition was possibly due to the formation of an unreactive water-TBA complex which decreased the fractional coverage of reactive adsorbed TBA. The formation of water-reactant dimer has also been reported for inhibiting the rates of alcohol dehydration.[3, 24] Lastly, the hypothesized cooperative adsorption theory was quantitatively verified by microkinetic modeling.

Based on the understanding achieved with water, we expect to extend the scope of research to other solvents and examine whether the proposed theory could be generally applicable. In this study, we tested twenty solvents varying in molecular size, polarity and proton affinity using similar strategy of TBA Hofmann elimination over H-ZSM-5 catalyst. Various degrees of inhibition were observed for different solvents, while kinetic and in-situ spectroscopic characterization revealed inhibition mechanism similar to water. In addition, a roughly linear relationship between degree of inhibition and solvent molecular dipole moment was observed, albeit exceptions exist, which indicated the solvent effect is likely related to strength of interaction between adsorbed solvent molecule with the Brønsted acidic proton of adsorbed TBA. Finally, due to the inaccuracy in predicting rate of Hofmann elimination in the presence of several solvents, an update was made on the cooperative adsorption theory that the formed solvent-TBA adsorption complex is also reactive towards Hofmann elimination but with a low rate constant. Non-linear regression results suggest that the observed inhibitory effect is likely due to a coupled effect by

the reactivity of solvent-TBA complex as well as the equilibrium constant of adsorption complex formation that dictates its fractional coverage on catalyst surface.

2. Experimental

2.1. Materials. Tert-Butylamine (TBA, ≥ 99.5%), hexane (≥ 99.5%), diethyl ether (inhibitor free, ≥ 99.9%), methanol (≥ 99.9%), 2-methyl-2-pentanol (99%), cyclohexanol (99%), acetonitrile (99.8%), and aniline (≥ 99.5%) were purchased from Sigma-Aldrich. Carbon dioxide (99.999%) was purchased from Airgas. Benzene (99%), 2,2,2-trichloroethanol (99%), 2-pentanol (99%), and 1-hexanol were purchased from Alfa Aesar. Ethanol (200 proof) was purchased from Decon Laboratories. 2-Fluoroethanol (95%), 2,2-difluoroethanol (> 98%), 2,2,2-trifluoroethanol (99.8%), 1-propanol (99.5%), 2-propanol (⩾ 99.9%), 1-butanol (99.9%), and 1,2-dichloroethane (⩾ 99%) were purchased from Thermo Fisher Scientific. Type 1 water (> 18.2 MΩ cm^{-1}) was obtained from laboratory water purification system. All liquid reagents, except for diethyl ether and aniline due to their instability in air at ambient condition, were dried with molecular sieves (3Å beads, 8-12 mesh, Sigma-Aldrich) overnight before use.

Ammonium form ZSM-5 (CBV2314, Si/Al = 11.5; CBV8014, Si/Al = 40; CBV28014, Si/Al = 140) were obtained from Zeolyst, and proton form ZSM-5 (Si/Al = 219) was obtained from Thermo Fisher Scientific.

2.2. Catalytic testing. Prior to loading into packed bed reactor, all zeolite catalysts were subjected to an ex-situ calcination to convert the zeolite to proton form, as well as sieving to obtain a reproducible particle size. The detailed experimental setup and procedures were discussed in our previous article.[23] Briefly, the catalyst was loaded in a 1/2" U-shape quartz tube, and a 1/16" type-K thermocouple (KQXL-116G-12, Omega) encased within a quartz sheath was placed in direct contact with the catalyst bed for temperature measurement. The catalyst was calcined at 823 K for 10 h with a ramp rate of 2 K min^{-1} in a tube furnace (GSL-1100X, MTI corporation) under a 100 sccm flow of air (Ultra-zero, Airgas) regulated by a mass flow controller (5850S, Brooks Instrument). The calcined catalyst powders were then pressed in a pellet press, crushed, and sieved to obtain a desired particle diameter. In all kinetic measurements, catalysts with particle diameter of 106 – 250 μm were used to minimize the intraparticle diffusion length while maintaining a low pressure drop across the catalyst bed.

Catalyst performances were tested in a custom-built packed bed reactor system. The catalyst was loaded in a 1/2" quartz downflow packed bed reactor (with shorter length than the one used in ex-situ calcination), resting on a plug of deactivated glass wool. The reactor was placed within a ceramic furnace, whose temperature was controlled using a PID temperature controller (CN 7823, Omega) that was used only for heating during pre-treatment. Both the quartz reactor and ceramic furnace were housed inside a larger forced convection oven (5890 Series II, HP) that controls the reactor temperature during reaction, which ensured the absence of temperature gradients across the reactor. The catalyst bed temperature was measured in-situ by placing a 1/16" thermocouple on top of the bed. The loaded catalysts were pre-treated by an in-situ calcination in 60 sccm air at 823 K for 4 h at a ramp rate of 5 K min^{-1}, and then cooled to reaction temperature under the same flow rate of air before the gas was switched to helium and ready for reaction.

Liquid phase chemicals were injected using a syringe pump (Masterflex EW-74905-04, Cole-Parmer) and air-tight glass syringes (Hamilton Company) to a vaporization section (SS-200-3, Swagelok) through a 1/16" PEEK capillary line (0.01" I.D., TPK110, Vici Valco) connected to a 1/16" stainless-steel capillary line (0.01" I.D., T50C10D, Vici Valco). Helium (99.999%, Airgas) was used as carrier gas for the vaporized chemicals, the flow rate of which was was adjusted by mass flow controllers (5850S, Brooks Instrument). In addition to the ex-situ drying of the TBA reactant, the vapor mixture (He+TBA) was dried in-situ by passing it through a bed of molecular sieve 3Å (regenerated daily at 493 K in 30 sccm of He). Prior to contacting TBA, He was purified by passing it through a moisture trap (22014, Restek), an oxygen trap (22010, Restek) and a liquid nitrogen cooled trap (in that order). The direction of vapor mixture towards either the reactor or the bypass path was controlled by a combination of 4-port switching valve (A24UWE, Vici Valco) and 6-port switching valve (A26UWE, Vici Valco). Prior to contacting with catalyst bed, all reactants were directed to the bypass path for at least 30 min to ensure a stable partial pressure. Reactor and bypass effluents were analyzed using an on-line gas chromatograph (7890B, Agilent) equipped with a HP-5 capillary column (19091J-413, Agilent) and a HP-PLOT Q Column (19091P-Q04, Agilent) connected to a flame ionization detector (FID). The transfer line between the reactor outlet and the gas chromatograph was resistively heated to 403 K to avoid any condensation using Nickel Chromium wire (8880K77, McMaster), insulated with a high-temperature wrap sleeving (6811A11, McMaster).

In our previous study on the effect of water over TBA Hofmann elimination, different concentrations of TBA/water solution were prepared and vaporized to yield controlled partial pressures of TBA and water. In this study, however, due to the limited solubility of TBA in multiple selected solvents, we decided to feed TBA and solvent separately. For rate measurement under dry condition, the stream containing only TBA was sent to the reactor while the stream containing solvent was sent to the vent. When measuring the reaction rate in the presence of solvent, the stream containing solvents was directed through a 3-way valve switched by a pneumatic actuator (SS- 43GXS4 -31D, Swagelok) to merge with the stream containing only TBA, and the combined flow was sent to the catalyst bed. The detailed illustration is included in the supporting information (Supporting information **Figure S1**).

All kinetic measurements were performed between 453 – 503 K at 1.3 bar of total pressure; pressure drop across the catalyst bed was maintained below 10% of total pressure. Unless otherwise noted, the weight hourly space velocity (WHSV) was controlled anywhere between 1.3 and 142 g TBA g cat^{-1} h^{-1} while maintaining differential conditions with respect to TBA (< 10% conversion). As calculated in our previous study, under all conditions tested, the attainable equilibrium conversion was greater than 99%.[23] All carbon balances closed to within ±10%. Unless otherwise noted, all errors were calculated at a 95% confidence interval. The site time yield (STY) of Hofmann elimination was calculated by normalizing the molar flow rate of isobutene (F_{iC4}) with the catalyst mass (m_{cat}) and Brønsted acid site density ($S_{Brønsted}$),

$$\mathrm{STY} = \frac{F_{iC_4}}{m_{cat} S_{Brønsted}} [=] \frac{\text{mol of isobutene produced}}{\text{mol of } H^+ \text{ s}} \quad (1)$$

2.3. Catalyst characterization. In-situ Fourier transform infrared (FT-IR) spectroscopy was employed to characterize the surface species and quantify coverage under reaction conditions, using a Bruker Tensor II spectrometer equipped with a DLaTGS detector and mid-infrared source. Spectra were collected between 1000 and 6000 cm^{-1} with a 4 cm^{-1} resolution, averaged over 64 scans and subtracted from a background spectrum. Thin self-supporting catalyst wafers were prepared by pressing 10 – 15 mg cm^{-2} of finely ground catalyst powder in a pellet press at 20 MPa of pressure for 15 minutes. The catalyst wafer was then transferred to a pellet holder and loaded into a custom-built temperature-controlled transmission cell, which was equipped with water-cooled CaF_2 windows and a set of three cartridge heaters for heating. The temperature of the cell was controlled using a PID temperature controller (CN 7823, Omega) and a 1/16" type-K thermocouple, and a second thermocouple inserted in a thermowell near the self-supporting wafer was used to measure the catalyst temperature. The catalyst was calcined in-situ (60 sccm ultra-zero air) at 673 K for 1 h at a ramp rate of 3 K min^{-1}, and cooled down to reaction temperature. Liquid phase probe molecules were injected through a 1/16" PEEK capillary line (0.01" I.D., TPK110, Vici Valco) using a syringe pump (Masterflex EW-74905-04, Cole-Parmer) and air-tight glass syringes (Hamilton Company), and vaporized in He stream inside a vaporization section. The vapor mixture was directed either to the bypass path or the heated transmission cell using a 6-port switching valve (A26UWE, Vici Valco) placed within a heated valve enclosure (HVEB, Vici Valco). Any tubing downstream of the vaporization section was additionally heat traced using resistively heated Nickel Chromium wire (8880K77, McMaster) to avoid condensation, insulated using a high-temperature wrap sleeving (6811A11, McMaster). The outlet of the transmission cell was also connected to an on-line gas chromatograph, in order to obtain simultaneous information of surface coverage and reaction rate.

In this study, the vibration frequencies of interest are two N-H vibrational modes associated with adsorbed tert-butylammonium at 1500 and 1609 cm^{-1}, and their integrated peak areas are used for quantifying the coverage of tert-butylammonium on zeolite surface.

2.4. Temperature programmed methods. Temperature programmed surface reaction (TPSR) experiments were performed in a packed bed reactor assembly using identical quartz reactor – ceramic furnace – GC oven design as described in Sec 2.2, but with simplified flow paths. Liquid-phase probe molecules were fed to a vaporization section (SS-400-4, Swagelok) through a 1/16″ PEEK capillary line (0.01″ I.D., TPK110, Vici Valco) using a syringe pump (Masterflex EW-74905-04, Cole-Parmer) and air-tight glass syringes (Hamilton Company). A set of three 2-way valves (SS-42GS4, Swagelok) were arranged to direct the vapor stream with probe molecule either bypass the reactor to quantified whether the required partial pressure is reached, or towards the catalyst bed for adsorption. A flow diagram of the TPSR reactor system is included in the supporting information (Supporting information **Figure S2**).

After calcination (same procedure as described in Sec 2.2), the catalyst surface was first saturated with TBA at 373 K by exposure to a stream containing 1.3 kPa of TBA in He (100 sccm) for 10 minutes, followed by purging with a pure stream of He for 4 h to remove any weakly adsorbed molecules. Once purged, the catalyst bed temperature was the linearly ramped to 773 K at 10 K min^{-1} under a 200 sccm stream of He. As discussed later in Sec. 3.4, the He stream flowing

through the catalyst bed during the ramp may contain a controlled partial pressure of selected solvent for testing the effect of solvent on the TPSR profile.

A quadrupole residual gas analyzer (RGA, XT200M, Extorr) was used as the on-line detector to quantify the desorbed species in the effluent stream with high time resolution (data collected per 7.5 s). To quantify the formed butene(s) and unreacted TBA desorbed, the intensities of fragments with m/z ratios of 56 and 58 were tracked, respectively. Since TBA also forms fragment with m/z ratio of 56, its contribution to the total intensity of m/z = 56 fragment was calibrated using vapor with controlled different partial pressures of TBA. It should be pointed out that for butenes, the fragment with maximal relative intensity is m/z = 41 whose signal was also tracked. However, its intensity was affected more heavily by the presence of TBA and cofed solvent than that of m/z = 56, and thus not used for analysis.

The corrected intensity of m/z = 56 fragment is calculated as

$$I_{m/z=56,\ corrected} = I_{m/z=56} - \eta \cdot I_{m/z=58} \quad (2)$$

where $I_{m/z\ =\ 56}$ and $I_{m/z\ =\ 58}$ are the intensities for fragment m/z = 56 and m/z = 58 after subtracting the respective baseline, and η is the calibration factor of TBA contribution on the intensity of m/z = 56. The normalized rate of butene(s) formation (Rate / $Rate_{max}$) during the temperature ramp are calculated by normalizing $I_{m/z\ =\ 56,\ corrected}$ against its maximum.

3. Results & Discussion.

3.1. Similar kinetic behavior between water and organic solvents. The main feature of the water solvation effect over TBA Hofmann elimination is the reversible rate inhibition without changing the surface fractional coverage of adsorbed tert-butylammonium or the intrinsic reaction energetic barrier, on which the cooperative adsorption model is based on. It is thus important to confirm whether solvents other than water show a similar kinetic effect, and whether the cooperative adsorption model is generally applicable.

Reversible inhibition of the rates of Hofmann elimination normalized by Brønsted acid sites (BAS) density in zeolite, i.e. the site time yields (STYs), were observed during the co-feed of acetonitrile (ACN, **Figure 1A**), methanol, 2-propanol (Supporting information **Figure S3**) and all other tested solvents with TBA, albeit with varying degrees of inhibition. Under the same reaction condition and partial pressure of solvent in the feed, water inhibited the STY by 53%, 2-propanol by 78%, and both acetonitrile and methanol inhibited the STY by about 90%. It is noted that for all the tested solvents, the rate of Hofmann elimination instantaneously decreased when the solvent was present in the feed stream. When switched back to the dry feed stream, in most cases (e.g. water, 2-propanol) the rate was rapidly restored to the initial level prior to solvent addition, while for other solvents (e.g. methanol) the rate was restored over an extended period of time. The difference in the kinetic behavior is likely related to the thermodynamics of solvent adsorption and interaction with adsorbed TBA; the significantly more exothermic solvent adsorption and interaction with TBA may result in higher desorption barrier and less readily re-adsorption, which display as prolonged solvent desorption.

Additionally, the competition between solvent molecule and TBA for Brønsted acid sites was investigated using in situ infrared (IR) characterization, as previously applied for the case of water. In brief, the integrated area of δ(NH) deformation modes of tert-butylammonium at 1500

cm^{-1} was tracked during the course of TBA and solvent addition to quantify the surface fractional coverage of adsorbed TBA under reaction condition. The IR measurement was conducted with cofed acetonitrile, and it was found that despite the greater STY inhibition induced by acetonitrile as compared to water, no observable change in the integrated area of δ(NH) was identified **(Figure 1A** and Supporting information **Figure S4**), indicating no competitive adsorption between acetonitrile and TBA over BASs under the reaction condition. Considering the greater degree of inhibition (STY / STY_{Dry} = 0.09 vs 0.56) and relatively high proton affinity (779 vs 691, kJ mol^{-1})[25] compared to water as well as the majority of tested solvents, we do not anticipate the presence of competitive adsorption for other solvents under the reaction conditions employed in this study.

Moreover, to ensure the observed solvent imposed-rate reduction was purely due to kinetic effect, we employed the Koros−Nowak criterion to examine any transport limitation, via identifying whether the reaction rate changes linearly with varying active site density. In the previous study, we showed that the measured STYs were within a factor of 2 difference at multiple Si/Al and reaction temperatures, signifying the absence of any transport limitation under dry condition.[23] In the presence of solvent, STYs measured at two Si/Al (11.5 and 140) varied within a factor of 2 (expect for 1-hexanol) over solvents with distinct molecular sizes and inhibitory effects (**Figure 1B**). The results indicated that the rate inhibition cannot be attributed to intrapore transport limitation of TBA caused by the presence of solvent, and that the diffusion of solvent molecules was unlikely hindered under the reaction condition. DFT computation by DeLuca and Hibbitts predicts that molecules with larger size than benzene, toluene and para-xylene (critical diameter = 6.6Å) would encounter significant higher diffusional restriction inside the straight and sinusoidal channel of MFI.[26] Since no solvent molecule tested in this study has significantly larger molecular diameter than benzene in the radial direction of micropore, the lack of transport limitation for various solvents is consistent with the computational prediction.

Lastly, the inhibitory effect of acetonitrile was measured at multiple reaction conditions. Through measurement of STYs of Hofmann elimination over three Si/Al (11.5, 140 and 219) at two different temperatures (473 and 503 K), it was observed that the degree of inhibition increased monotonically with increasing partial pressure of acetonitrile and was independent of Si/Al of zeolite. A similar profile was observed at a higher temperature but with less degree of inhibition **(Figure 1C)**. Also, the STY of Hofmann elimination in the presence of acetonitrile or 2-propanol exhibited a zeroth-order dependence on the partial pressure of TBA, and identical kinetic profile was observed for water in our previous investigation **(Figure 1D**). Combined with the reversible rate inhibition behavior and lack of competitive adsorption against TBA, we thus believe that the tested solvents interact with adsorbed TBA over zeolite surface in a similar manner with water, that is, through the formation of unreactive solvent-TBA adsorption complex over the BAS as we proposed.

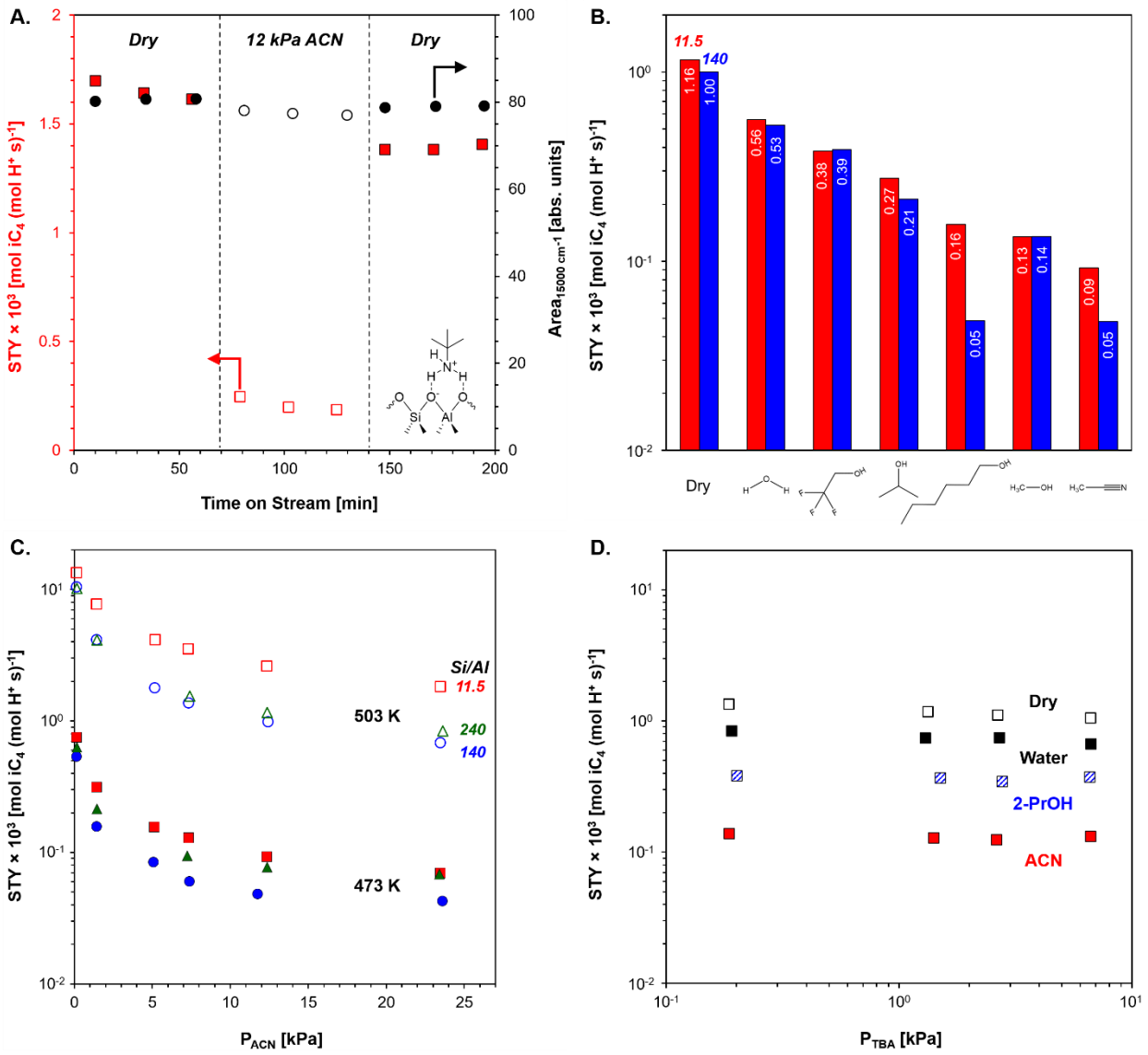

Figure 1. A. Site time yield (STY) of Hofmann elimination (■ / □) and the corresponding infrared integrated area of the tert-butylammonium δ(NH) deformation mode (1500 cm^{-1}, ● / ○) versus time on stream in the presence (unfilled) and absence (filled) of 12 kPa of acetonitrile. P_{TBA} = 1.3 kPa, T = 473 K, Si/Al = 11.5 **B.** STYs of Hofmann elimination in the presence of selected solvents over Si/Al = 11.5 (red) and 140 (blue). P_{TBA} = 1.3 kPa, $P_{Solvent}$ = 12 kPa, T = 473 K **C.** STYs of Hofmann elimination in the presence of acetonitrile, P_{TBA} = 1.3 kPa, P_{ACN} = 0.14 – 23 kPa, Si/Al = 11.5 – 219, T = 473 and 503 K **D.** TBA partial pressure dependence of STY under dry condition (□), in the presence of water (■), 2-propanol (2-PrOH, ▨) or acetonitrile (ACN, ■). Si/Al = 11.5, $P_{Solvent}$ = 7.3 kPa, T = 473 K.

3.2. Inhibitory effect by various solvents. With the assumption that all tested molecules solvate the Hofmann elimination with the same mechanism, we could then systematically investigate factors that dictate the degree of inhibitory effect. More than 20 solvents were tested for the kinetic effect over TBA Hofmann elimination, which cover a wide span of categories (nonpolar, polar aprotic and polar protic) and molecular properties (proton affinity, molecular dipole moment, dielectric constant of bulk liquid). Rates of Hofmann elimination were measured with identical partial pressures (P_{TBA} = 1.3 kPa and $P_{Solvent}$ = 12 kPa) at identical condition (T = 473 K). The properties of solvent, measured STYs and ratios with STY under dry condition are listed in **Table 1**. The criteria for the selection of solvents are that they do not react with TBA under the reaction condition (absence of side product was confirmed by on-line GC), or potentially competitively adsorb over the BAS (determined by the solvent proton affinity and confirmed by in situ IR).

A roughly linear trend is observed between STYs of Hofmann elimination and solvents' molecular dipole moments (**Figure 2**), as well as dielectric constants of bulk liquid solvent with the exception of water (Supporting information **Figure S5A**). Both dipole moment and dielectric constant are common descriptors for evaluating polarity of solvent, and the effects of solvent polarity on zeolite catalysis have been revealed in multiple previous investigations. Ristanović and coworkers reported a lower turnover frequency (by more than two orders of magnitude) for the H-ZSM-5 catalyzed oligomerization of 4-methoxystyrene in the solution of 1-butanol versus in n-heptane.[27] The authors proposed that the difference in reaction kinetics was due to the more pronounced competitive adsorption of the polar 1-butanol over Brønsted acid sites against reactant molecules. In another study, Gould et al. observed a trend for liquid-phase pyridine protonation by Brønsted acid sites in zeolite, which becomes less favorable with increasing solvent dielectric constant (1,4-dioxane > acetonitrile > water).[28] The greater stabilization of proton by water cluster compared to acetonitrile dimer was attributed for the variation in proton transfer equilibrium constant. However, in our case a greater rate inhibition of Hofmann elimination was observed with acetonitrile than water, which might be due to the Brønsted acidic proton not being shared between adsorbed TBA and solvent molecule. In general, we believe the trend with polarity reveals a correlation between the degree of solvent's inhibitory effect and the strength of interaction with the Brønsted acidic proton. Nonpolar solvents adsorb weakly and create weak electrostatic interaction with adsorbed tert-butylammonium, resulting in insignificant solvation effect, while highly polar solvents could cause stronger interaction with tert-butylammonium and more pronounced inhibitions on reaction rate.

Based on our proposed mechanism of solvating the Brønsted acidic proton, it is intuitive to hypothesize that gas phase basicity, as described by proton affinity, can also directly influence the extent of interaction between solvent and the Brønsted proton. Investigation by Nicholas demonstrated that the proton affinity of acetone adsorbed over H-ZSM-5 is significantly promoted upon the co-adsorption of a solvent molecule such as nitromethane, facilitating the proton transfer from Brønsted site to adsorbed acetone.[29] However, in the case of Hofmann elimination, no observable trend is found between the degree of inhibition and solvent proton affinity (Supporting information **Figure S5B**).

It should be emphasized that there are still multiple points of STYs, mainly the alcohols, fall outside the linear trend with molecular dipole moment, which suggests that dipole moment is

unlikely the sole descriptors for the solvent effect and there could be multiple factors determining the kinetics. On the other hand, the values of molecular dipole moment used in this study are from experimental measurements for gas phase monomer. However, the dipole moment of polar molecules, water included, can be significantly enhanced under the effects of polarization and delocalization through, for example, hydrogen bond formation in water clusters and condensed phases.[30] In contrast, under confined environment the number of hydrogen bonds decreases compared to the bulk liquid and such enhancement in dipole moment of water cluster/network is attenuated.[31, 32] Additionally, water possesses much higher bulk liquid dielectric constant than other solvents (as shows in **Table 1** and **Figure S4A**), while several recent publications have showed that the dielectric constant of polar molecules could dramatically decrease by up to two orders of magnitude under highly confined environment.[33, 34] Therefore, it should be emphasized that the values of solvent molecular properties listed in **Table 1** do not represent their true values under zeolite microporous confinement at reaction conditions (which is difficult to measure or predict accurately), but serve as semi-quantitative indication of a relative trend in polarities of different solvents.

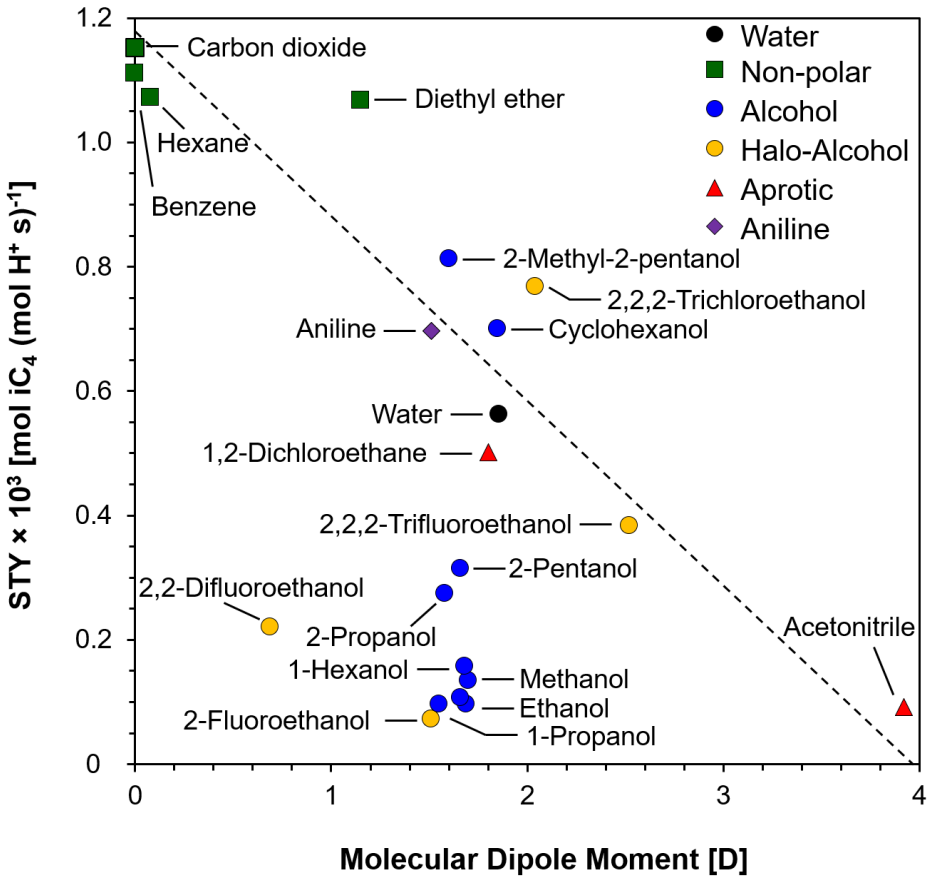

Figure 2. Relationship between STYs of Hofmann elimination and solvent molecular dipole moments. Si/Al = 11.5, P_{TBA} = 1.3 kPa, $P_{Solvent}$ = 12 kPa, T = 473 K. The dashed line is for eye-guiding purpose only.

Table 1. TBA Hofmann elimination over H-ZSM-5 in the presence of solvents, Si/Al = 11.5, P_{TBA} = 1.3 kPa, $P_{Solvent}$ = 12 kPa, T = 473 K.

Solvent	Category	Proton affinity [kJ mol^{-1}]	Molecular dipole moment [D]	Bulk dielectric constant	STY ×10^3 [mol iC_4 (mol H^+ s)$^{-1}$]	STY / STY_{Dry}
Dry					1.16	1.00
Carbon dioxide	Non-polar	540[a]	0[e]	1.0[e]	1.15	0.99
Hexane	Non-polar	672[b]	0.08[f]	1.9[e]	1.07	0.92
Water	Non-polar	691[a]	1.85[e]	80.1[e]	0.56	0.47
Benzene	Non-polar	750[a]	0[g]	2.3[e]	1.11	0.92
Diethyl ether	Non-polar	828[a]	1.15[e]	4.3[e]	1.07	0.84
Methanol	Polar Protic	754[a]	1.70[e]	33.0[e]	0.13	0.09
Ethanol	Polar Protic	776[a]	1.69[e]	25.3[e]	0.10	0.08
2-Fluoroethanol	Polar Protic	716[a]	1.51[h]	N.A.[l]	0.07	0.06
2,2-Difluoroethanol	Polar Protic	727[a]	0.69[i]	N.A.[l]	0.22	0.17
2,2,2-Trifluoroethanol	Polar Protic	700[a]	2.52[f]	27.7[e]	0.38	0.30
2,2,2-Trichloroethanol	Polar Protic	729[a]	2.04[j]	N.A.[l]	0.77	0.60
1-Propanol	Polar Protic	787[a]	1.55[e]	20.8[e]	0.10	0.07
2-Propanol	Polar Protic	793[a]	1.58[e]	20.2[e]	0.27	0.22
1-Butanol	Polar Protic	789[a]	1.66[e]	17.8[e]	0.11	0.08
2-Pentanol	Polar Protic	815[a]	1.66[e]	13.7[m]	0.31	0.24
1-Hexanol	Polar Protic	799[a]	1.68[k]	13.0[e]	0.16	0.11
Cyclohexanol	Polar Protic	787[c]	1.85[f]	16.4[e]	0.70	0.54
2-Methyl-2-pentanol	Polar Protic	803[a]	1.60[f]	5.8[e]	0.81	0.65
Aniline	Polar Protic	883[a]	1.53[f]	7.1[e]	0.70	0.56
Acetonitrile	Polar Aprotic	779[a]	3.92[e]	36.6[e]	0.09	0.08
1,2-Dichloroethane	Polar Aprotic	628[d]	1.8[e]	10.4[e]	0.50	0.40

a. Ref. 25
b. Ref. 35
c. Ref. 4
d. Ref. 36. Value is not available, assumed to be identical with dichloromethane
e. Ref. 37
f. Value from www.stenutz.eu
g. Ref. 38
h. Ref. 39
i. Ref. 40
j. Ref. 41
k. Ref. 42
l. Not available
m. Ref. 43

3.3. Solvent effect of alcohols.

3.3.1 Aliphatic Alcohols.

It is noticed that primary aliphatic alcohols deviate most significantly from the trend between reaction STYs and solvent dipole moments, and thus it is important to perform a deeper investigation on what caused such deviation. For C1 to C6 primary alcohols, identical inhibitory effect was observed regardless of the alkyl chain length (**Figure 3A**). The insensitivity in reaction STY in the presence of alcohols with varying carbon number is inconsistent with the work by Torres et al., in which the rate of 1-hexene epoxidation differs by two orders of magnitude over silanol-rich Ti-incorporated MFI.[16] They attributed the variation in turnover rate with alkyl chain length to the different densities of hydrogen bond network, and the decrease in entropic gain that results from the disruption of hydrogen bonds by reactant molecules and subsequent reorganization of solvent structure. In contrast, the absence of rate dependence on alcohol carbon number in our study might be due to TBA possessing much stronger hydrogen-bonding ability than the relatively non-polar 1-hexene. As both strong hydrogen-bond donor and acceptor, the presence of TBA may not effectively change the hydrogen bond network of alcohol inside the micropore, and thus the reaction entropic gain does not have a strong dependence on the length of alkyl chain. We also plotted the STY of Hofmann elimination against a hydrogen-bond acceptor descriptor, pK_{BHX},[44] over multiple tested solvents to evaluate the relationship with the strength of hydrogen-bonding (Supporting information **Figure S6**), but no observable trend was found, indicating the hydrogen-bonding ability of solvent does not directly correlate to the macroscopic kinetics. The similar STY in the presence of 1-hexanol with methanol or ethanol also indicates the absence of diffusional limitation inside the micropore for the longer alkyl chain, which is consistent with the result of Koros−Nowak test in Sec. 3.1.

Moreover, **Figure 3A** shows a trend of decreasing degree of STY inhibition with increasingly substituted α-carbon on primary, secondary (2-propanol, 2-pentanol, cyclohexanol) and tertiary alcohols (2-methyl-2-pentanol). It is immediately noticed that this trend of increasing STY somehow coincides with the increasing carbocation stability of the α-carbon due to hyperconjugation, and the same mechanism that increases the electron density on the α-carbon may destabilize the interaction between adsorbed alcohol and neighboring tert-butylammonium and lead to weaker inhibitory effect. Among the secondary alcohols, cyclohexanol exhibits less inhibition compared to the noncyclic 2-propanol and 2-pentanol. Since steric hindrance is unlikely to explain the difference as revealed by the similar STYs between 2-propanol and 2-pentanol (also between methanol and 1-hexanol), one potential explanation is that the cyclic ring induced additional destabilization due to the proximity of more alkyl groups to the α-carbon than the linear alkyl chain.

To quantitatively verify the hypothesis, we plotted the STY of Hofmann elimination in the presence of solvent against the values of hydride ion affinity (HIA) which is traditionally used to evaluate the stability of carbocation.[45, 46] A strong negative correlation between the reaction STY and HIA of alcohols was observed, indicating the validity of the hypothesis (Supporting information **Figure S7**). However, it is also noticed that methanol exhibits similar inhibitory effect with ethanol, despite methyl cation being much less stable than ethyl cation as indicated by its significantly higher HIA value. One possibility for the inconsistency is that methanol is slightly

more acidic than ethanol (the effect of acidity will be discussed in the next section) as indicated by a lower proton affinity, which weakens the interaction with adsorbed tert-butylammonium.

It should be mentioned that all aliphatic alcohols undergo dehydration reaction when co-fed with TBA over the zeolite catalysts, as the corresponding alkene and ether products were detected by on-line GC. The dehydration rates, however, are more than three orders of magnitude lower compared with feed of pure alcohol at identical reaction condition and alcohol partial pressure in the feed stream (Supporting information **Figure S8**). Since the surface BASs are irreversibly saturated with adsorbed TBA, the active site for alcohol dehydration is likely being the Lewis acidic extra-framework aluminum. The low alcohol dehydration activity is consistent with the low concentrations of extra-framework aluminum in commercial MFI zeolites (less than 20%)[47] and lower alcohol dehydration activity over Lewis acid sites.[48]

3.3.2 Halogen-substituted Alcohols

Halogen-substituted alcohols, with varying halogen element and number of halogen substituents, exhibit similar dipole moment but different proton affinities. In addition, 2,2,2-trifluoroethanol is commonly used as a polar solvent in organic syntheses.[49-51] These features make halogen-substituted ethanols interesting for systematically probing the solvation effect.

For fluorine-substituted ethanol, the STY of Hofmann elimination is similar between ethanol and mono-substituted ethanol, but becomes significantly higher with two and three F atoms on the β-carbon (**Figure 3B**). The decreasing degree of inhibition is against the rationalization based on carbocation stability, since the presence of neighboring electron-withdrawing group (CH_mF_n) will destabilize the carbocation[52] and would lead to a reverse trend of STY with number of F atom (lower STY with more F atoms) if the same mechanism holds. On the other hand, the electronegative F atom could withdraw electron density from the terminal OH group and thus increase the acidic character of the OH group, as shows by the significantly lower gas-phase basicity and pK_a values of F-substituted ethanols than unsubstituted ethanol (**Table 2**). It is possible that the higher acidity of the OH group makes the interaction with the Brønsted acidic proton of tert-butylammonium less favorable due to charge repulsion, resulting in less effective solvation.

In addition, a higher STY of Hofmann elimination was observed with 2,2,2-trichloroethanol as compared with the fluoro-counterpart. The OH group of 2,2,2-trichloroethanol is expected to have a lower acidity due to the less electronegative Cl atom than F atom, which is consistent with its higher gas-phase basicity. The lower inhibitory effect induced by a less acidic molecule contradicts the proposed rationalization. Possible explanations include steric hindrance between the micropore wall and the larger Cl atoms preventing the most preferred configuration for the interaction between adsorbed 2,2,2-trichloroethanol and tert-butylammonium. Alternatively, the proximity of Cl atoms to the micropore wall may lead to stronger van der Waals interaction, and introducing additional electron-withdrawing effect that further increases the acidity of the terminal OH group.

Overall, there could be multiple factors that affect the strength of interaction between adsorbed TBA and neighboring solvent molecules. Currently no solid conclusion can be made on why we observed a near-linear trend with dipole moment and why it fails for multiple alcohols, but these investigations may offer guidance for directing the next step of study.

Table 2. Acidity parameters for ethanol and halogen-substituted ethanols.

Solvent	Proton affinity [kJ mol^{-1}]	Gas-phase basicity [kJ mol^{-1}]	pK$_a$
Ethanol	776[a]	746[a]	15.5[b]
2-Fluoroethanol	716[a]	685[a]	N.A.
2,2-Difluoroethanol	727[a]	697[a]	N.A.
2,2,2-Trifluoroethanol	700[a]	670[a]	12.37[b]
2,2,2-Trichloroethanol	729[a]	699[a]	12.24[b]

a. Ref. 25
b. T = 298 K, Ref. 37

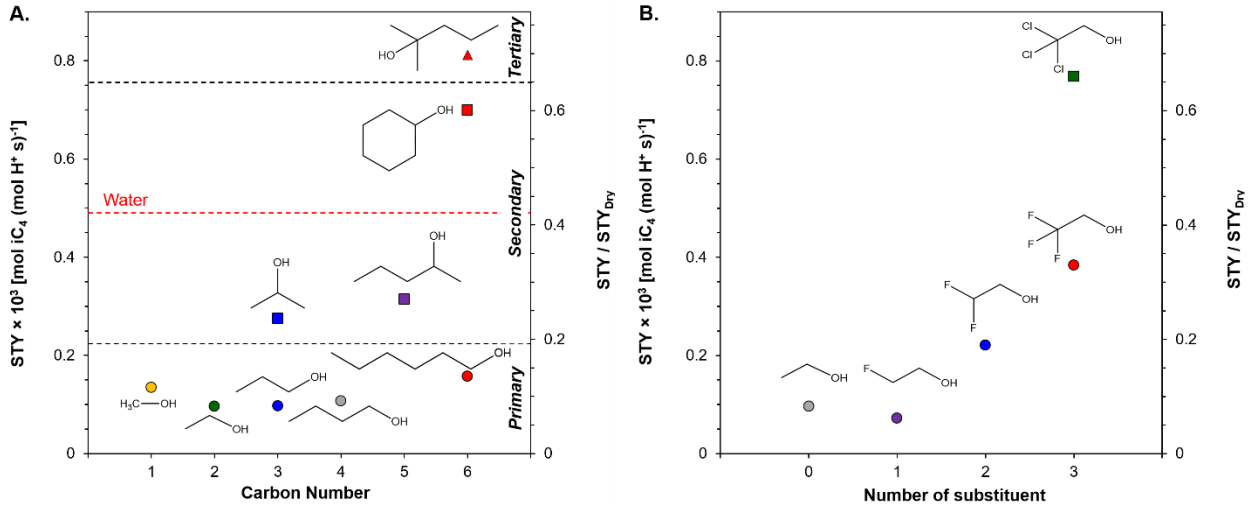

Figure 3. STYs of Hofmann elimination in the presence of **A.** aliphatic alcohols with varying carbon numbers, and **B.** halogen-substituted ethanols with varying numbers of halogen substituent. Si/Al = 11.5, P_{TBA} = 1.3 kPa, $P_{Solvent}$ = 12 kPa, T = 473 K.

3.4. Energetics of cooperative adsorption. We have compared the solvation effect of solvents across a wide range of polarity and basicity, which is based on the hypothesis that all solvents tested would interact with adsorbed tert-butylammonium in a similar way as water through the formation of cooperative adsorption complex. Two major findings from previous study which laid the foundation of cooperative adsorption theory is that the intrinsic reaction barrier of Hofmann elimination is not altered in the presence of water, as well as water adsorbs unimolecularly over the adsorption site and interacts with adsorbed TBA. To make an appropriate comparison of solvation effect based on cooperative adsorption mechanism, it is necessary to confirm whether the two observations from previous study remain valid for different solvents.

Previously we showed that in the presence of 24 kPa of water, the apparent activation energy of Hofmann elimination increased by ~ 30 kJ mol^{-1}, from 174 kJ mol^{-1} to 203 kJ mol^{-1} at 453 – 493 K. However, a combination of temperature-programmed surface reaction (TPSR) and

kinetic modeling revealed that the increase in apparent value was not due to contribution from intrinsic reaction barrier, but instead the enthalpy of water adsorption and surface coverage of water-TBA complex.

In this study, similar increases in apparent activation energy, measured in the same temperature range, were observed in the presence of acetonitrile and methanol (213 and 192 kJ mol^{-1}, respectively, **Figure 4A**), although at a much lower content of 1.3 kPa. The similar increase in apparent activation energy at a significantly lower solvent partial pressure indicates that, if cooperative adsorption theory applies, either the enthalpy of solvent adsorption is much higher than that of water, or the fraction coverage of solvent-TBA complex is similar despite a much lower partial pressure. Both possibilities lead to a stronger interaction with adsorbed TBA and thus a greater rate inhibition compared with water, which is consistent with the kinetic measurement results. TPSR was also performed in the presence of acetonitrile and methanol to verify any change in the energetics of the rate-determining step. The accuracy of TPSR method was previously confirmed by the well-predicted peak temperature in the absence of water by first-order Polanyi−Wigner equation. With 1.3 kPa of acetonitrile being constantly fed during the temperature ramp, the peak temperature of the TPSR curve (T_{Peak}) increased by 7 K (**Figure 4B**), which corresponds to a 3 kJ mol^{-1} increase in activation barrier based on a Redhead analysis, as opposed to ~ 40 kJ mol^{-1} increase in apparent activation energy. Similarly, a slight shift of 2 K in T_{Peak} was observed in the presence of 1.3 kPa of methanol, which corresponds to only 1 kJ mol^{-1} decrease in activation energy. Additionally, for a TBA-saturated catalyst, treating the catalyst by flowing 1.3 kPa of acetonitrile for 30 min before the temperature ramp (no feed during the ramp) did not alter the peak temperature (Supporting information **Figure S9**). If the 20 – 40 kJ mol^{-1} change in apparent activation energy was due to an increase in intrinsic reaction barrier of Hofmann elimination, a shift towards higher temperature by ~56 – 110 K in T_{Peak} would have been observed. The absence of such drastic change of TPSR peak temperature indicates the absence of a change in intrinsic barrier of Hofmann elimination even under stronger solvation effect induced by acetonitrile or methanol.

3.5. Update on cooperative adsorption model. To verify whether the cooperative adsorption kinetic model previously proposed for water is generally applicable for various solvents, as well as to examine any underlying defect in the model, we applied the model to multiple tested solvents and made comparison with the experimental results. As shows by the parity plots (Supporting information **Figure S10**), the model was able to capture the kinetic trend for 2-propanol over a span of three orders of magnitude, but for acetonitrile and methanol deviations from the experimental data were observed, which indicates that the elementary steps of the current model might not be able to comprehensively describe the catalytic cycle in the presence of solvent.

Therefore, we closely reviewed our model and attempt to find what could be causing the inaccuracy. A central assumption of the cooperative adsorption theory is that the formed solvent-TBA adsorption complex is completely unreactive towards Hofmann elimination, which appears to be valid for the case of water. Alternatively, we speculated that the adsorption complex might be relatively unreactive compared with parent tert-butylammonium, but still has a non-zero rate constant. To quantitatively verify this hypothesis, the STY expression for Hofmann elimination is defined based on the updated elementary steps with one additional step showing the conversion of

solvent-TBA adsorption complex (Step 6). In addition, it is possible that depending on the nature of the solvent, the solvent molecule could interact with the adsorbed tert-butylammonium in the form of dimer, trimer, or an extended network, leading to different structures of adsorption complex. Therefore, the adsorption stoichiometries n is proposed to indicate the number of solvent molecules involved in the formation of solvent-TBA complex per BAS.

Table 3. Updated elementary steps for Hofmann elimination, with Step 6 showing the reaction of solvent-TBA adsorption complex.

	Elementary Step
1	$TBA + * \rightleftharpoons TBA_*$
2	$TBA_* \rightleftharpoons iC_{4*} + NH_3$
3	$iC_4 + * \rightleftharpoons iC_{4*}$
4	$NH_3 + * \rightleftharpoons NH_{3*}$
5	$nS + TBA_* \rightleftharpoons nS\text{-}TBA_*$
6	$nS\text{-}TBA_* \rightleftharpoons iC_{4*} + NH_3 + nS$

Based on the updated elementary steps, the expression of STY becomes

$$STY = \frac{r}{S_{Brønsted}} = \frac{k_2 K_{TBA} P_{TBA} + k_6 K_{Solvent} K_{TBA} P_{Solvent}^n P_{TBA}}{(1 + K_{TBA} P_{TBA} + K_{Solvent} K_{TBA} P_{Solvent}^n P_{TBA})} \quad (3)$$

Where k_2 and k_6 are the forward kinetic rate constants for adsorbed TBA and solvent-TBA complex, respectively. The regression of the previous model showed a lack of sensitivity for K_{TBA} (in terms of $\Delta H_{ads,TBA}$ and $\Delta S_{ads,TBA}$)and also $K_{TBA}P_{TBA} \gg 1$, which is consistent with the saturation of TBA over the BASs regardless of reaction conditions. Thus, simplification of **eq 3** by assuming $K_{TBA}P_{TBA} + K_{TBA}K_{Solvent}P_{TBA}P_{Solvent}^n \gg 1$ yields

$$\frac{r}{S_{Brønsted}} \approx \frac{k_2 + k_6 K_{Solvent} P_{Solvent}^n}{(1 + K_{Solvent} P_{Solvent}^n)} \quad (4)$$

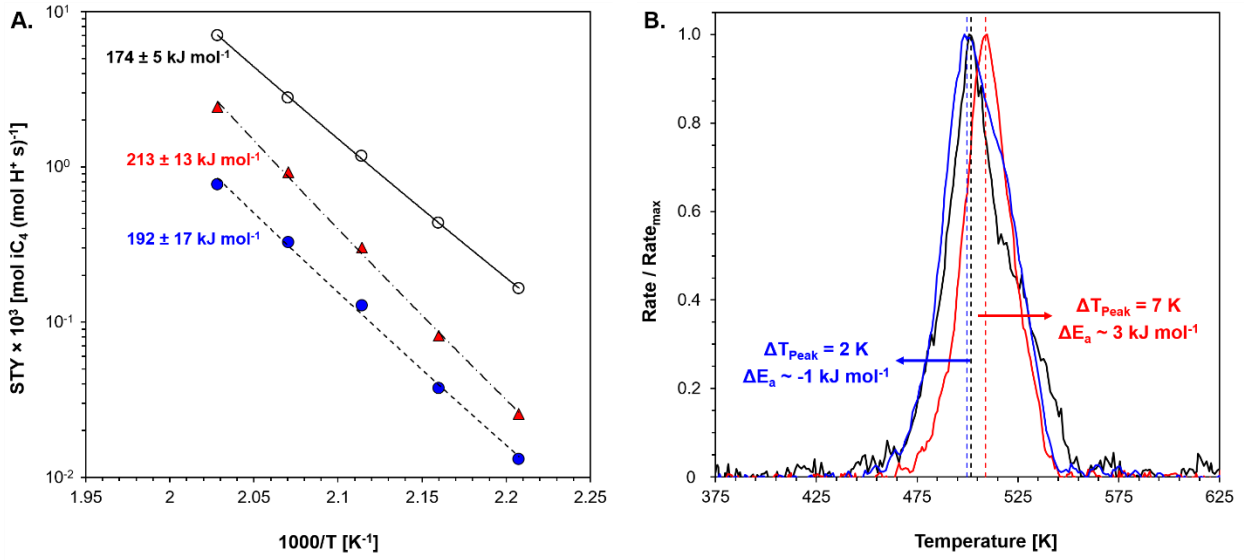

Figure 4. A. Activation energies of TBA Hofmann elimination in the environment of dry TBA (○), 1.3 kPa of acetonitrile (▲) and 1.3 kPa of methanol (●). Si/Al = 11.5, T = 453 – 493 K **B.** TPSR profile of pre-adsorbed TBA over H-ZSM-5 Si/Al = 219 in the absence (black) and presence of 1.3 kPa of acetonitrile (red) or methanol (blue) between 373 and 773 K, with a 10 K min^{-1} ramp rate.

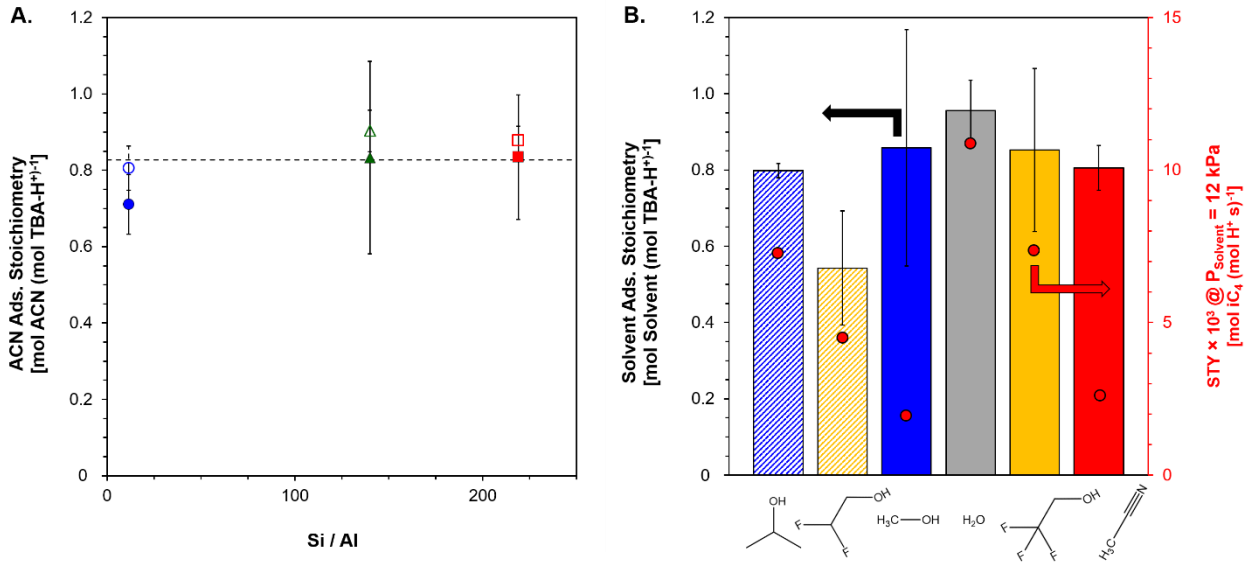

Figure 5. A. Adsorption stoichiometry of acetonitrile based on regression of the updated cooperative adsorption model over Si/Al = 11.5 (● / ○), 140 (▲ / △), and 219 (■ / □) at T = 473 K (filled) and 503 K (unfilled) **B.** Adsorption stoichiometries of selected solvents and the corresponding STYs in the presence of 12 kPa of solvent. Si/Al = 11.5, T = 503 K.

To validate the model and obtain an image of the structure of adsorption complex, it is important to first quantify the number of solvent molecules involved in the solvent-TBA complex formation. Computation of adsorption stoichiometries was performed through non-linear regression in MATLAB. Over a wide range of acetonitrile partial pressure (0.14 – 24 kPa), Si/Al (11.5, 140, 219) and temperature (473 and 503 K), the regressed adsorption stoichiometry of acetonitrile n is found to be independent of Si/Al and reaction temperature, with an average value of 0.8 (**Figure 5A**). Although it is arguable that n < 1 could physically suggest that one solvent molecule is shared between two neighboring BASs, which is more likely occurring over zeolite with a high Al content due to a higher concentration of paired sites,[53] the identical n over zeolites of Si/Al = 11.5 and 219 contrast to this interpretation, as the distance between neighboring BASs should be distinctly different considering the drastically different BAS densities. The insensitivity of kinetic behavior of acetonitrile with respect to Si/Al (as showed in **Figure 1C**) also indicates the hypothesis of shared solvent molecule between sites is unlikely. Therefore, we believe that the true stoichiometry should equal to 1 during the adsorption of ACN. This unimolecular adsorption of acetonitrile per BAS, being insensitive to Si/Al and reaction temperature, is also consistent with the general acknowledgement that acetonitrile does not form cluster or hydrogen-bonding network.[28, 54] It is envisioned that one acetonitrile molecule adsorbs on the framework oxygen neighboring the Brønsted acidic proton and interact with it with the -C≡N terminal group. The strong ion-dipole interaction effectively stabilizes the formed acetonitrile-TBA adsorption complex and results in a pronounced solvation effect of inhibiting the Hofmann elimination reaction.

Since the adsorption stoichiometry n = 1 was also observed in the case of water,[23] we were interested in the adsorption of other solvents. **Figure 5B** shows that for six selected solvents, within experimental error the regressed n at 503 K are all approximately 1. It is noted that no clear relationship was found between the calculated n and the solvent property descriptor such as molecular dipole moment, nor with the measured STYs of reaction in the presence of 12 kPa of solvent. Based on the results, we conclude that for all solvents tested in this study, they would form solvent-TBA dimer upon their adsorption on the framework oxygen neighboring the tert-butylammonium, whether their interaction with the tert-butylammonium is weak or strong. The degree of kinetic inhibition is determined by the thermodynamic and kinetic properties of the solvent-TBA dimer, rather than the different structures of solvent-TBA adsorption complex (e.g. solvent clusters or networks for more inhibiting solvents or at higher partial pressures).

Consequently, with n = 1 **eq 4** becomes

$$\frac{r_{Solvent}}{S_{Brønsted}} = \frac{k_2 + k_6 K_{Solvent} P_{Solvent}}{(1 + K_{Solvent} P_{Solvent})} \tag{5}$$

Divided by the rate expression under dry condition (**eq 6**) gives the expression for the ratios of STY / STY_{Dry} which indicates the degree of solvent inhibitory effect

$$STY_{Dry} = \frac{r_{Dry}}{S_{Brønsted}} = \frac{k_2 K_{TBA} P_{TBA}}{(1 + K_{TBA} P_{TBA})} \approx k_2 \tag{6}$$

$$\frac{STY}{STY_{Dry}} = \frac{r}{r_{Dry}} = \frac{1 + \frac{k_6}{k_2} K_{Solvent} P_{Solvent}}{(1 + K_{Solvent} P_{Solvent})} \tag{7}$$

Therefore, the updated kinetic model can be regressed with only two parameters, the ratio of rate constants for decomposition of adsorbed solvent-TBA complex and neat tert-butylammonium k_6 / k_2, as well as the equilibrium constant of solvent-TBA complex formation $K_{Solvent}$.

Figure 6A and **6B** displays the comparison between the experimentally measured ratios of STY (symbols) and the fitted results for selected solvents (curves) at 503 K. Results at 473 K are showed in Supporting information **Figure S11** – **S13**. The kinetic trends of various solvents over more than three orders of magnitudes of STY were clearly better predicted than the previous model assuming solvent-TBA complex completely unreactive. The regressed values of k_6 / k_2 and $K_{Solvent}$ are summarized in **Table 4**. Across all solvents tested, the regressed k_6 values are consistently lower than 20% of k_2, while the values of $K_{Solvent}$ vary over three orders of magnitude. A higher k_6 indicates a more reactive adsorption complex, and a higher $K_{Solvent}$ indicates more favorable formation of adsorption complex (more negative $\Delta G_{Solvent}$) and thus higher surface coverage. In the presence of water, the regressed rate constant for water-TBA complex k_6 is only 6% of that for tert-butylammonium under dry condition (k_2), which is trivial and explains why it is reasonable to assume the adsorption complex is unreactive in our previous model. Also, since k_2 is the rate constant of the adsorbed tert-butylammonium and is associated with the intrinsic kinetics of TBA Hofmann elimination, its value should not be dependent on the solvent environment. Using the ΔH (168 kJ mol^{-1}) and ΔS of activation (50 J mol^{-1} K^{-1}) obtained from our last article,[23] we calculate the k_2 and corresponding k_6 under reaction conditions (Supporting information **Table S3**).

The fitted equilibrium constant $K_{Solvent}$ in the presence of water is also consistent with the value regressed previously (10.6 vs 6.8), confirming the accuracy of the updated model. Additionally, $K_{Solvent}$ are consistently lower (except for methanol which could be due to error in STY measurement) at a higher temperature which indicates the exothermic nature of adsorption complex formation. The lower $K_{Solvent}$ at a higher temperature also suggest lower coverages of solvent-TBA complex, which are consistent with the observed decreased rate inhibitions observed at an elevated temperature. To further quantify the thermodynamic properties involved, we calculated the enthalpies and entropies of solvent-TBA complex formation using the regressed values of $K_{Solvent}$. According to Dauenhauer and Abdelrahman,[55] the entropy of adsorption for a mobile adsorbate over MFI zeolite is approximately the combination of the entropy of one degree of translational and rotational entropic freedom. Similar to the adsorption of solvent molecule over the zeolite surface, the formation of solvent-TBA complex also involves hydrogen bonding and the formed adsorption complex is also likely a mobile adsorbate. Therefore, we assume the entropy of solvent-TBA complex formation ($\Delta S_{Solvent}$) is similar the entropy of solvent adsorption over MFI, and accordingly we can calculate the enthalpy of formation ($\Delta H_{Solvent}$) using the fitted $K_{Solvent}$ (Supporting information **Table S4**). It is noticed that methanol possesses both the highest $K_{Solvent}$ and the most exothermic formation of adsorption complex with TBA among solvents fitted with the updated model. The high $K_{Solvent}$ suggests a favorable formation of methanol-TBA complex that could be accountable for the observed longer time of STY restoring to the initial level after methanol was removed from the feed stream, as methanol slowly desorbed from the surface.

Lastly, to gain a deeper understanding on the effect of solvent and factors that determining the energetics of solvation, the relationship between the fitted parameters and solvent property

descriptors were investigated. Surprisingly, no obvious trend was found between solvent molecular dipole moments and the regressed values of $K_{Solvent}$ or k_6 / k_2 (Supporting information **Figure S11**), despite the trend with apparent reaction STY. On the other hand, a volcano-shaped profile was observed between solvent proton affinity and $K_{Solvent}$ (with the maximum being with methanol), while the k_6 / k_2 remain roughly constant around 0.1 across the range of proton affinity (**Figure 6C** and **Figure S12**). It is noticed that the trends of calculated $\Delta H_{Solvent}$ as well as $\Delta S_{Solvent}$ against proton affinity are much less significant as compared with $K_{Solvent}$, which could due to the compensation between enthalpic and entropic contributions (Supporting information **Figure S14**). The influence of solvent proton affinity on $K_{Solvent}$ potentially reflect how the formation of solvent-TBA complex is affected by the strength of interaction between adsorbed solvent and Brønsted acidic proton within tert-butylammonium: for solvent with a low proton affinity (low basicity), the weak bonding with proton leads to an unstable adsorption complex; for solvent with a high proton affinity (high basicity), the strong interaction with proton may lead to weakening of N-H bond and ultimately abstraction of proton and desorption of TBA (although not observed in this study). Both leads to decreased coverage of solvent-TBA adsorption complex over the zeolite surface.

In summary, the lack of dependence of k_6 / k_2 on neither solvent molecular dipole moment or proton affinity indicates that the reactivity of solvent-TBA complex towards Hofmann elimination is large unaffected by the identity of solvent molecule. Since the intrinsic barrier of Hofmann elimination is not altered as shows by the TPSR results in Sec. 3.4, it is unlikely that the rate-determining step of Hofmann elimination would be changed by the presence of different solvents. In contrast, the varying degree of observed rate inhibition is mainly determined by the difference in the thermodynamics of solvent-TBA complex formation via changing the surface coverage of adsorption complex, as the equilibrium constant of solvent-TBA complex formation being seemingly correlated with solvent proton affinity. It should be pointed out the proposed microscopic relationship still cannot explain why the absence of a clear trend between the macroscopic STY of Hofmann elimination and solvent proton affinity, which manifests the complicated nature of solvation of BAS that cannot be quantified by a single descriptor. Since the choice of solvent molecular properties in this article (i.e. dipole moment, dielectric constant and proton affinity) are arbitrary, there could be other parameters that could also be involved in describing the solvent effect, as we have pointed out earlier.

Table 4. Fitted parameters from regression of the updated model

Solvent	Temperature [K]	k_6 / k_2	$K_{Solvent}$
Water	473	0.06	10.6
	503	0.04	3.2
Methanol	473	0.10	2632.1
	503	0.12	2668.6
2-Propanol	473	0.08	40.7
	503	0.15	13.9
Acetonitrile	473	0.05	228.9
	503	0.07	73.5
2,2-Difluoroethanol	473	0.14	169.9
	503	0.19	86.0
2,2,2-Trifluoroethanol	473	0.18	45.3
	503	0.09	11.8

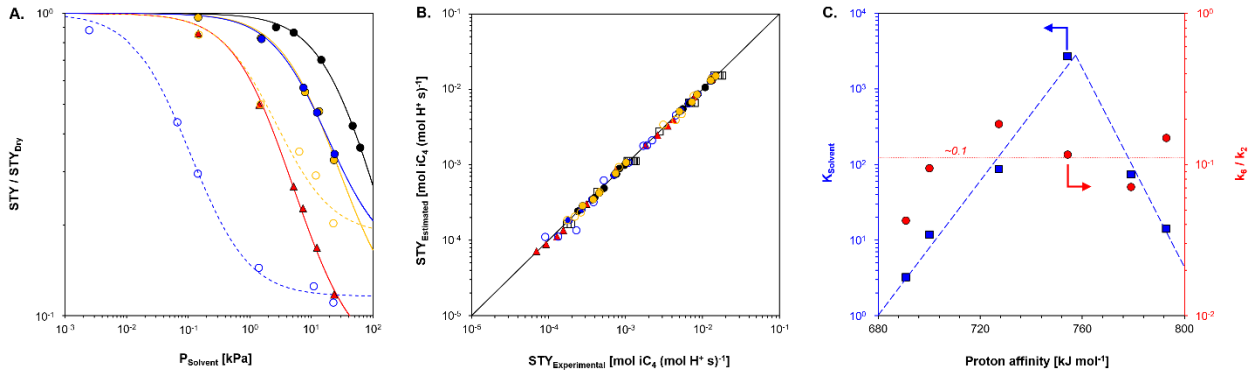

Figure 6. Regression of the updated cooperative adsorption kinetic model. **A.** Ratios of STY (STY / STY_{Dry}) at varying solvent partial pressures: water (●), methanol (○), 2-propanol (●), acetonitrile (▲), 2,2-difluoroethanol (○), 2,2,2-trifluoroethanol (●). Symbols represent experimentally measured data and curve represent fitting using the fitted parameter set in **Table 4**. Si/Al = 11.5, $P_{Solvent}$ = 0.002 – 63 kPa, T = 503 K **B.** Parity plot comparing the predicted and experimentally measured STYs of TBA Hofmann elimination showed in panel **A** plus STYs measured under dry condition (□) from ref. 23 **C.** Relationship between fitted $K_{Solvent}$ and k_6 / k_2 with proton affinity of corresponding solvent, T = 503 K. Dashed lines are for eye-guiding purpose only.

4. Conclusion. Using the gas phase Hofmann elimination of tert-butylamine as probe chemistry, the kinetic effect on solvation of Brønsted acid sites in aluminosilicate zeolites were investigated with multiple solvents commonly used in organic reactions. 21 solvents occupying a wide range of molecular dipole moment, bulk liquid dielectric constant and proton affinity were selected for testing their impacts on the reaction site time yield. All solvents were able to reversibly decrease

the catalytic activity towards Hofmann elimination, the degree of which appears to be positively correlated with the molecular dipole moment of solvent in a rough shape. Even in the presence of a highly inhibitive solvent such as acetonitrile (reducing STY by more than 90%), the surface coverage of adsorbed tert-butylammonium and the intrinsic reaction barrier remained unchanged. A systematic investigation on the effect of alcohols and halogen-substituted alcohols revealed that with increasing number of alkyl group substitution on α-carbon as well as terminal halogen atom on β-carbon, the extent of kinetic inhibition is reduced. Lastly, an additional elementary step of the cooperative adsorption theory hypothesizing an adsorption complex formed between solvent molecule and TBA over Brønsted acid site being reactive towards Hofmann elimination were proposed, which was quantitatively verified through kinetic modeling. It was found that with the formation of solvent-TBA dimer over a wide range of conditions, the equilibrium constant of dimer formation shows a maximum against the proton affinity of solvents, while the ratios of rate constant for solvent-TBA complex and tert-butylammonium undergoing elimination remain relatively unchanged among different tested solvents.

Supporting Information. Details of the experimental setup, kinetic measurement of TBA Hofmann elimination in the presence of selected solvents, FT-IR spectra of adsorbed TBA over H-ZSM-5 in the presence of solvent, relationship between STY of TBA Hofmann elimination and pK_{BHX} and hydride ion affinity, relationship between fitted $K_{Solvent}$ and k_6 / k_2 and solvent molecular dipole moment and proton affinity are available in the supporting information.

Acknowledgements. We acknowledge support from the Catalysis Center for Energy Innovation, an Energy Frontier Research Center funded by the U.S. Department of Energy, Office of Science, Office of Basic Energy Sciences under Award number DE-SC0001004.

References

1. R. Bermejo-Deval, R. S. Assary, E. Nikolla, M. Moliner, Y. Román-Leshkov, S.-J. Hwang, A. Palsdottir, D. Silverman, R. F. Lobo, L. A. Curtiss and M. E. Davis, *Proceedings of the National Academy of Sciences*, 2012, **109**, 9727-9732.
2. R. Bermejo-Deval, R. Gounder and M. E. Davis, *ACS Catal.*, 2012, **2**, 2705-2713.
3. Y. Zhi, H. Shi, L. Mu, Y. Liu, D. Mei, D. M. Camaioni and J. A. Lercher, *J. Am. Chem. Soc.*, 2015, **137**, 15781-15794.
4. Y. Liu, A. Vjunov, H. Shi, S. Eckstein, D. M. Camaioni, D. Mei, E. Baráth and J. A. Lercher, *Nature Communications*, 2017, **8**, 14113.
5. L. Zhang, T. N. Pham, J. Faria and D. E. Resasco, *Appl. Catal., A*, 2015, **504**, 119-129.
6. H.-K. Min, S. H. Cha and S. B. Hong, *ACS Catal.*, 2012, **2**, 971-981.
7. D. T. Bregante, A. M. Johnson, A. Y. Patel, E. Z. Ayla, M. J. Cordon, B. C. Bukowski, J. Greeley, R. Gounder and D. W. Flaherty, *J. Am. Chem. Soc.*, 2019, **141**, 7302-7319.
8. G. Li, B. Wang, B. Chen and D. E. Resasco, *J. Catal.*, 2019, **377**, 245-254.
9. E. M. Erenburg, T. V. Andrushkevich, G. Y. Popova, A. A. Davydov and V. M. Bondareva, *React. Kinet. Catal. Lett.*, 1979, **12**, 5-11.
10. C. J. Gilbert, J. S. Espindola, W. C. Conner Jr, J. O. Trierweiler and G. W. Huber, *ChemCatChem*, 2014, **6**, 2497-2500.

11. J. S. Bates, B. C. Bukowski, J. Greeley and R. Gounder, *Chem. Sci.*, 2020, **11**, 7102-7122.
12. M. A. Mellmer, C. Sener, J. M. R. Gallo, J. S. Luterbacher, D. M. Alonso and J. A. Dumesic, 2014, **53**, 11872-11875.
13. C. Aellig and I. Hermans, *ChemSusChem*, 2012, **5**, 1737-1742.
14. E. Nikolla, Y. Román-Leshkov, M. Moliner and M. E. Davis, *ACS Catal.*, 2011, **1**, 408-410.
15. N. M. Bertero, A. F. Trasarti, M. C. Acevedo, A. J. Marchi and C. R. Apesteguía, *Molecular Catalysis*, 2020, **481**, 110192.
16. C. Torres, D. S. Potts and D. W. Flaherty, *ACS Catal.*, 2023, **13**, 8925-8942.
17. A. K. Chew, T. W. Walker, Z. Shen, B. Demir, L. Witteman, J. Euclide, G. W. Huber, J. A. Dumesic and R. C. Van Lehn, *ACS Catal.*, 2020, **10**, 1679-1691.
18. V. L. Sushkevich and J. A. van Bokhoven, *Catal. Sci. Technol.*, 2020, **10**, 382-390.
19. F. Cavani, G. Girotti and G. Terzoni, *Appl. Catal., A*, 1993, **97**, 177-196.
20. S. M. T. Almutairi, B. Mezari, E. A. Pidko, P. C. M. M. Magusin and E. J. M. Hensen, *J. Catal.*, 2013, **307**, 194-203.
21. C. Sievers, Y. Noda, L. Qi, E. M. Albuquerque, R. M. Rioux and S. L. Scott, *ACS Catal.*, 2016, **6**, 8286-8307.
22. M. J. Cordon, J. N. Hall, J. W. Harris, J. S. Bates, S.-J. Hwang and R. Gounder, *Catal. Sci. Technol.*, 2019, **9**, 1654-1668.
23. H. Chen and O. A. Abdelrahman, *ACS Catal.*, 2021, **11**, 6416-6430.
24. J. R. Di Iorio, A. J. Hoffman, C. T. Nimlos, S. Nystrom, D. Hibbitts and R. Gounder, *J. Catal.*, 2019, **380**, 161-177.
25. E. P. L. Hunter and S. G. Lias, *Journal of Physical and Chemical Reference Data*, 1998, **27**, 413-656.
26. M. DeLuca and D. Hibbitts, *Microporous Mesoporous Mater.*, 2022, **333**, 111705.
27. Z. Ristanović, A. V. Kubarev, J. Hofkens, M. B. J. Roeffaers and B. M. Weckhuysen, *J. Am. Chem. Soc.*, 2016, **138**, 13586-13596.
28. N. S. Gould, S. Li, H. J. Cho, H. Landfield, S. Caratzoulas, D. Vlachos, P. Bai and B. Xu, *Nature Communications*, 2020, **11**, 1060.
29. J. B. Nicholas, *Top. Catal.*, 1999, **9**, 181-189.
30. T. Zhu and T. Van Voorhis, *The Journal of Physical Chemistry Letters*, 2021, **12**, 6-12.
31. C. Liang, A. Rayabharam and N. R. Aluru, *J. Phys. Chem. B*, 2023, **127**, 6532-6542.
32. C. Dellago and M. M. Naor, *Computer Physics Communications*, 2005, **169**, 36-39.
33. P. Loche, C. Ayaz, A. Wolde-Kidan, A. Schlaich and R. R. Netz, *J. Phys. Chem. B*, 2020, **124**, 4365-4371.
34. M. H. Motevaselian and N. R. Aluru, *ACS Nano*, 2020, **14**, 12761-12770.
35. K. C. Hunter and A. L. L. East, *J. Phys. Chem. A*, 2002, **106**, 1346-1356.
36. F. Cacace, G. d. Petris, F. Pepi, M. Rosi and A. Troiani, *Chem. Eur. J.*, 1999, **5**, 2750-2756.
37. D. R. Lide, *CRC Handbook of Chemistry and Physics*, CRC Press, Internet Version 2005 edn., 2005.
38. A. A. Maryott and F. Buckley, *Table of Dielectric Constants and Electric Dipole Moments of Substances in the Gaseous State*, U.S. Department of Commerce, National Bureau of Standards, 1953.
39. K. S. Buckton and R. G. Azrak, *The Journal of Chemical Physics*, 2003, **52**, 5652-5655.

40. K.-M. Marstokk and H. Møllendal, *Acta Chemica Scandinavica*, 1980, **34**, 765-770.
41. S. S. .Krishnamurthy and S. Soundararajan, *J. Phys. Chem.*, 1969, **73**, 4036-4039.
42. V. A. Rana and H. A. Chaube, *Journal of Molecular Liquids*, 2013, **187**, 66-73.
43. C. Wohlfarth, in *Landolt-Börnstein - Group IV Physical Chemistry* ed. M. D. Lechner, Springer-Verlag Berlin Heidelberg, vol. 17, ch. Static Dielectric Constants of Pure Liquids and Binary Liquid Mixtures (Supplement to IV/6).
44. C. Laurence, K. A. Brameld, J. Graton, J.-Y. Le Questel and E. Renault, *Journal of Medicinal Chemistry*, 2009, **52**, 4073-4086.
45. D. H. Aue and M. T. Bowers, in *Gas Phase Ion Chemistry*, ed. M. T. Bowers, Academic Press, 1979, DOI: https://doi.org/10.1016/B978-0-12-120802-8.50007-2, pp. 1-51.
46. D. W. Berman, V. Anicich and J. L. Beauchamp, *J. Am. Chem. Soc.*, 1979, **101**, 1239-1248.
47. O. A. Abdelrahman, K. P. Vinter, L. Ren, D. Xu, R. J. Gorte, M. Tsapatsis and P. J. Dauenhauer, *Catal. Sci. Technol.*, 2017, **7**, 3831-3841.
48. C. P. Nash, A. Ramanathan, D. A. Ruddy, M. Behl, E. Gjersing, M. Griffin, H. Zhu, B. Subramaniam, J. A. Schaidle and J. E. Hensley, *Appl. Catal., A*, 2016, **510**, 110-124.
49. K. S. Ravikumar, V. Kesavan, B. Crousse, D. Bonnet-Delpon and J.-P. Bégué, *Org. Synth.*, 2003, **80**, 184-189.
50. B. Milani, A. Anzilutti, L. Vicentini, A. Sessanta o Santi, E. Zangrando, S. Geremia and G. Mestroni, *Organometallics*, 1997, **16**, 5064-5075.
51. Siu M. Ng, C. Yin, Chi H. Yeung, Tak C. Chan and Chak P. Lau, *European Journal of Inorganic Chemistry*, 2004, **2004**, 1788-1793.
52. T. T. Tidwell, *Angewandte Chemie International Edition in English*, 1984, **23**, 20-32.
53. A. Lawal and O. A. Abdelrahman, *J. Phys. Chem. C*, 2023, **127**, 20857-20869.
54. R. Brakaspathy and S. Singh, *Journal of Chemical Sciences*, 1986, **96**, 285-290.
55. P. J. Dauenhauer and O. A. Abdelrahman, *ACS Cent. Sci.*, 2018, **4**, 1235-1243.